In Situ Structure of Intestinal Apical Surface Reveals Nanovilli on Microvilli

Hao Zhu (zhuh17@mails.tsinghua.edu.cn)
Tsinghua University
Meijing Li
Tsinghua University
Ruixue Zhao
Tsinghua University
Ming Li
National Institute of Biological Sciences, Beijing https://orcid.org/0000-0003-4137-5290
Zhaodi Jiang
1. PTN Graduate Program, School of Life Sciences, Tsinghua University 2. National Institute of Biological Sciences, Beijing
Yongping Chai
Tsinghua University
Zhiwen Zhu
Tsinghua University
Yihong Yang
Tsinghua University
Wei Li
Tsinghua University
Zhongyun Xie
Tsinghua University
Xiaomin Li
Tsinghua University
Kexin Lei
Tsinghua University
Wanzhong He
National Institute of Biological Sciences, Beijing https://orcid.org/0000-0001-7367-9868
Xueming Li
Tsinghua University
Guangshuo Ou
Tsinghua-Peking Center for Life Sciences, Beijing Frontier Research Center for Biological Structure, School of Life Sciences and MOE Key Laboratory for Protein Science, Tsinghua University, Beijing

Letter

Keywords: microvilli, C. elegans , nanovilli

Posted Date: April 19th, 2021

DOI: https://doi.org/10.21203/rs.3.rs-398232/v1

Abstract

Microvilli are actin bundle-supported membrane protrusions essential for absorption, secretion, and sensation. Microvilli defects cause human diseases, including gastrointestinal disorders and inherited deafness; however, mechanisms controlling microvilli formation and organization remain unclear. Here, we study microvilli by vitrifying the *C. elegans* larvae and mouse intestinal tissues with high-pressure freezing, thinning them by cryo-focused ion beam milling, cryo-electron tomography, and sub-tomogram averaging. We uncover that hundreds of previously unrecognized stick-like structures, which we refer to as nanovilli, decorate the lateral surface of *C. elegans* and mouse microvilli. The *C. elegans* 37.5-nm long and 4.5-nm wide nanovilli are composed of the protocadherin family protein CDH-8. Loss of nanovilli slows down animal growth and increases the number of Y-shaped microvilli, intermediate structures when a microvillus splits from its tip and separates into two. Our results show that nanovilli space microvilli and suggest a microvilli division model through which microvilli assemble with striking uniformity.

Introduction

The architecture of the cell surface is crucial for metazoan development and physiological homeostasis. Microvilli are membrane-bound cell surface protrusions that contain a core bundle of actin filaments enveloped in the plasma membrane [1-3]. Many epithelial cells develop this organelle above their apical surface to enhance functional capacity for a range of physiological tasks, including nutrient absorption in the intestine [4], solute uptake in the renal tubules [5], mechanosensation in sensory stereocilia of the inner ear [6], and chemosensation in the gut, lung, and urogenital tracts [7-9]. Abnormal microvillar structure and function lead to human disorders such as life-threatening nutrient malabsorption and osmatic imbalances and inherited deafness in Usher syndrome [1,3,4,10].

An intestinal enterocyte develops up to one thousand densely packed microvilli in an array known as the "brush border" (BB). These fingerlike outward projections enhance the functional surface area for nutrient absorption and provide the barrier for host defense against pathogens and toxins [1,3,4]. Despite their importance, we know little about how microvilli are formed with striking uniformity in sizes and how these protrusions are maximally packed in a hexagonal pattern. Because the gut epithelium undergoes the constant regenerative renewal, microvillus assembly is a process that continues throughout our lifetime [1,3,4,11]. However, an individual microvillus is only 0.1 μm in diameter and ~2 μm in height (Fig. 1a), the tiny size of which, along with their high density and lumen localization, becomes a technical hurdle for *in situ* structural investigations at high resolution [1-3].

Cryo-ET of *C. elegans* larvae

Recent methodology advance of cryo-electron tomography (cryo-ET) makes the platform well suited to address the challenges of studying microvillus structure in animals [12,13]. As a proof-of-concept, we initiated the cryo-ET study of intestinal microvilli in the nematode *Caenorhabditis elegans*. Classical

transmission electron microscopy (TEM) documented the anatomy and molecular organization of the *C. elegans* intestine and microvilli, which highly resemble those in mammals, supporting the notion that microvilli are evolutionarily conserved organelles (Fig. 1a, Extended Data Fig. 1a) [14,15]. Studies of microvilli in other species require tissue dissection or *in vitro* cell culture systems. In contrast, the thickness of the *C. elegans* L1 larvae, which is approximately 12.5 μm in diameter (Extended Data Fig. 1a) [14,15], allows high-pressure freezing (HPF) of an entire animal, thereby enabling structural analysis of microvilli in their close-to-native conditions.

We employed cryo-focused ion beam milling (cryo-FIB) to produce thin lamellas from the frozen-hydrated vitrified worms [12]. By taking advantage of the invariance of the *C. elegans* gut development and anatomy [14,15], we focused on the intestine from the newly hatched first-stage juvenile (L1 larva, 6 hours after hatching). The larval intestine runs approximately 70% of body length between the anterior pharynx and the posterior hindgut [14,15]. We thinned the intestine's central region, approximately 150 μm posterior from the animal's nose, corresponding to the intestinal cells from Int4 to Int7 (Fig. 1b, Extended Data Fig. 1a and Supplementary Video 1). Cryo-FIB milling removed the biological material above and below the area, generating a 150- to 200-nm-thick cellular lamella traversing the whole animal with high consistency and reproductivity (Fig. 1b). Next, we applied cryo-ET to image the cryo-lamella, which facilitates the three-dimensional (3D) visualization of microvilli at unprecedented molecular resolution. Each lamella provided a suitable imaging area of ~10×10 μm^2, from which we obtained 2~3 cryo-ET tilt series. In agreement with the early TEM observations [14,15], our tomograms of the *C. elegans* microvilli revealed that the plasma membrane surrounds the actin bundles in the core (Fig. 1c, Supplementary Video 1). The plasma membrane appears as two smooth and parallel black lines, and actin bundles from the cross-section were resolved as individual black dots (Fig. 1d, Supplementary Video 1). The excellent contrast and rich structural details from the reconstructed tomogram demonstrate the high quality of prepared samples (Fig. 1d, Supplementary Video 1).

Discovery of nanovilli from *C. elegans* intestine

Strikingly, we found hundreds of stick-like structures projecting out from each microvillus's lateral surface (Fig. 1c,f and Supplementary Video 2). These structures are highly uniform, with a constant diameter of 4.5 ± 0.5 nm (n = 4, 983 mean ± SD). They appear to be the transmembrane structure whose extracellular length is 37.5 ± 0.2 nm (mean ± SD). Each tomographic slice contains 50 ± 5 (mean ± SD, from 12 focal planes) of the stick-like structures (Fig. 1d, e), highlighting their abundance. These structures are distinct from the glycoprotein-rich glycocalyx, a region between the apical tip of microvilli and the luminal space (Fig. 1a), which provides a barrier for pathogens and serves as the interface for nutrient digestion [3,4]. These sticks are also different from protocadherin-based adhesion tip links between adjacent microvilli, which only localize at microvillar tips (Fig. 1a) [16]. By contrast, the stick-like structures distribute along the lateral surface of microvilli (Fig. 1c, f). Microvilli are considered tiny micrometer appendages that decorate the epithelium surface, and our results reveal that these previously unrecognized yet highly

abundant nanometer attachments further decorate microvilli's lateral surface. Therefore, we have named a single stick-like structure nanovillus because of its size and location relative to microvillus.

We wondered why the previous TEM studies did not describe nanovillus. The TEM sample preparation involves chemical fixation, dehydration, and heavy metal staining, which are not compatible with high-resolution structural studies. Although TEM cannot resolve an individual nanovillus, this technique may detect an electron-dense layer that contains numerous nanovilli at the lateral surface of microvilli. To test this idea, we performed TEM of HPF, freeze-substituted *C. elegans*. We determined an excellent TEM quality microvillus if the plasma membrane's lipid bilayer is resolved as two parallel black lines. From such microvilli, we indeed found an electron-dense area along microvilli's lateral surface from either longitudinal or cross-sections (Fig. 2a). The thickness of these layers is 37.3 ± 0.5 nm (51 nanovilli layers from 3 animals, mean ± SD) (Fig. 2a), comparable to that of cryo-ET tomograms. We noticed a thin band that does not have electron density localized between two adjacent nanovilli layers (Fig. 2a). Such electron transparent bands indicate the separation of nanovilli layers and suggest that nanovilli might be involved in intermicrovillar spacing.

Nanovilli in mouse intestine

We asked whether mammals develop a similar nanovilli structure on microvilli. First, we screened the published TEM images of microvilli. Most of the sample preparation relied upon chemical fixation, which did not yield high-quality pictures on the microvillar membrane. Considering that membrane preservation is probably a prerequisite to visualize the fine structure on its surface, we performed HPF and freeze-substituted mouse intestinal tissues, allowing the visualization of a lipid bilayer in the microvillar membrane as two black lines (Fig. 2b). We detected a similar electron-dense layer on the lateral surface of mouse microvilli in the longitudinal or cross-sections (Fig. 2b). Next, we employed the same cryo-FIB milling and cryo-ET platform that detects *C. elegans* nanovilli to examine mouse intestinal tissues. In agreement with our TEM results, 13.8 ± 0.8 nm long stick-like structures decorate the lateral surface of mouse microvilli (64 mouse nanovilli from 4 tomograms, mean ± SD) (Fig. 2c). Despite the difference in length, these stick-like structures' morphology and location suggest that nanovilli, like microvilli, might be widespread from nematodes to mammals.

Nanovillus formation requires CDH-8

We sought to identify the molecular composition of nanovilli. We performed single-cell mRNA sequencing of *C. elegans* larvae to gain insights into the intestine transcriptome (Extended Data Fig. 1b, c, Table s1, details in Materials and Methods). A previous study documented the proteome of the mouse brush border [17]. Among the overlapped hits between the *C. elegans* intestinal transcriptome and mouse brush border proteome, the intriguing candidates are the protocadherin family proteins (Extended Data Fig. 1d, and 2a). The transmembrane protocadherin family proteins mediate cell-cell adhesion, such as PCDH24 and PCDH15 in the intermicrovillar link at microvillar tips [3,16,18,19]. however, an electron transparent band between two adjacent microvilli indicates that nanovilli layers are not linked but well separated (Fig. 2a).

Considering that the mouse protocadherin 8 protein plays a repulsive role in mediating the dendritic self-avoidance during neural development [20,21], we asked whether protocadherin might be a component of nanovilli.

We obtained the protocadherin *cdh-3*, *cdh-8*, and *cdh-10* mutant alleles defective in *C. elegans* protocadherin genes to probe this possibility. Because TEM offers the throughput to screen for the nanovilli layer and electron-transparent intermicrovillar band, we used this method to assess nanovilli in multiple mutants quickly. The nanovilli and transparent bands in *cdh-3* and *cdh-10* deletion mutants are indistinguishable from those in *wild-type (WT)* animals (Fig. 2d, > 200 examined microvilli from three animals of each genotype). By contrast, we did not detect the nanovilli layer or the electron transparent band in *cdh-8(ok628)* mutant animals (530 examined microvilli from five animals), despite excellent preservation of the microvillar membrane (Fig. 2d). Our cryo-ET tomograms further confirmed the loss of nanovilli in *cdh-8(ok628)* animals. We occasionally found stick-like structures between microvilli in *cdh-8(ok628)* mutants (Fig. 3c, yellow arrows), but their more prolonged length (56.8 ± 5.4 nm, n =50, mean ± SD, versus 37.5-nm-long nanovilli) indicates that they are distinct structures from nanovilli.

Protocadherin genes are well-known for their alternative splicing [21], and the *cdh-8(ok628)* allele has an in-frame deletion that removes 119 residues in its extracellular domain (Fig. 2e). To rule out the effects of a large variety of protocadherin isoforms, we implemented the CRISPR-Cas9-based homologous recombination strategy to precisely remove the transmembrane domain along with the entire intracellular domain of CDH-8, which are shared by all the CDH-8 isoforms, generating a *cdh-8(cas1109)* mutant allele (Fig. 2e). Our TEM datasets uncovered that the nanovilli layer and the electron transparent band disappeared in *cdh-8(cas1109)* mutants (Fig. 2d, 365 examined microvilli from 4 animals). The cryo-ET pipeline also revealed the loss of nanovilli in *cdh-8(cas1109)* animals (Fig. 3a-f and Supplementary Video 3-5). Our results from two mutant strains show that CDH-8 is essential for nanovilli formation.

To define the molecular architecture of nanovilli, we performed unbiased subtomogram averaging of nanovilli from cryo-ET datasets. A total of 4983 nanovilli were hand-picked from 11 tomograms, aligned, and averaged to produce an average structure (Fig. 3g, h). While the resolution did not allow us to speculate the molecular composition of nanovilli, the density map shows that a single nanovillus compromises nine repeats in the extracellular domain, the transmembrane region, and the intracellular domain (Fig. 3g, h). Consistently, CDH-8 is predicted to consist of nine extracellular cadherin (EC) domains, a single transmembrane (TM) helix, and an intracellular domain (Fig. 3g, h). X-ray crystallography characterized the atomic resolution structures of EC domains [22]. Using its characteristic curvature, we manually fitted nine copies of the human protocadherin-15's EC8 domain (PDB code 4XHZ) into the nanovillus extracellular region of our sub-tomogram averaging structure (Fig. 3h and Supplementary Video 6), further supporting the molecular connection between CDH-8 and nanovilli.

Consistent with the structural results, our GFP-based transcriptional reporter indicated that the *cdh-8* gene was expressed in the *C. elegans* intestinal cells (Extended Data Fig. 2b), validating our single-cell sequencing data. We expressed the GFP-tagged CDH-8 full-length protein in the *C. elegans* intestinal cells.

By constructing a red fluorescence protein mScarlet knock-in animal to label an established microvillus marker ERM-1 (the Ezrin/Radixin/Moesin family protein) [2,3], we showed the colocalization of the green CDH-8::GFP and the red ERM-1::mScarlet fluorescence in the intestinal lumen (Extended Data Fig. 2c), providing evidence that CDH-8 is the component of nanovilli.

Loss of Nanovilli slows down animal growth

Next, we used the *cdh-8* mutant animals to dissect the function of nanovilli. We did not notice any apparent defects in the overall animal morphology or the number of progenies; however, our quantifications of the body length at each developmental stage revealed a reduction of animal growth in *cdh-8* mutant animals (Extended Data Fig. 3a). Because the eggshell prevents embryos from accessing the bacterial food, our measurements started from the newly hatched larvae, when the worm body lengths are indistinguishable between *cdh-8* mutants and *WT*. With the progression of animal growth in the presence of the same food, the body lengths of *cdh-8* mutant alleles were shorter than that of *WT* animals at the various larval stages (Extended Data Fig. 3a). At 122 hours after hatching, when *C. elegans* already developed into the day two adults, *cdh-8* deletion animals reached the *WT* body length (Extended Data Fig. 3a). Notably, the GFP-tagged *cdh-8* gene expression using an intestinal-specific promoter P*ges-1* fully rescued the slow growth phenotype in both *cdh-8* mutant alleles (Extended Data Fig. 3b), demonstrating a cell-autonomous function of *cdh-8* in promoting animal growth. These data indicate that nanovilli function from the *C. elegans* intestine to regulate animal growth. We suggest that the growth delay might result from the less efficient food update and that the slow but continuous growth eventually restored the *cdh-8* mutant body length to the *WT* level.

Y-shaped microvilli and the role of nanovilli in spacing microvilli

To address if nanovilli contribute to microvilli assembly and organization, we compared microvilli structure in *cdh-8* mutant and *WT* animals. Our TEM analyses detected the forked or branched (collectively called Y-shaped) microvilli in *cdh-8* mutant animals with 4% (*ok628*, 530 microvilli from 5 animals) or 16% (*cas1109*, 351 microvilli from 4 animals) penetrance (Fig. 4a). The Y-shaped microvilli were rarely detectable in *WT* animals (Fig. 4a, 468 microvilli from 5 animals); neither did our literature search find Y-shaped microvilli under the standard conditions. Curiously, half a century ago, the Y-shaped microvilli were described during the salamander microvilli regeneration (Extended Data Fig. 2d) [23]. Using hydrostatic pressure to eliminate microvilli on the small intestine, Tilney and Cardell observed the Y-shaped regenerating microvilli four minutes after pressure release but not later on, suggesting that Y-shaped microvilli might represent an intermediate structure during microvilli regeneration.

In a developing *WT C. elegans* larva, one of the cryo-ET tomograms showed a Y-shaped microvillus with two separated tips but a single base (Fig. 4b, c, and Supplementary Video 7). Consistent with our TEM results, we only detected one Y-shaped microvillus from more than 100 examined ones, which indicates the occurrence of such a structure during animal development and suggests that a Y-shaped microvillus might be transient. In *cdh-8* mutant animals, the Y-shaped microvilli may be an arrested status of a

splitting microvillus; and the lack of nanovilli failed to space two daughter microvilli efficiently, thereby enriching Y-shaped microvilli (Fig. 4a). Unlike the straight nanovilli on the well-spaced microvilli, nanovilli on the newly split microvilli were bent (red sticks in Fig. 4c lower), implying that nanovilli straightening might push two nascent microvilli apart. In support of this idea, loss of nanovilli markedly reduced the distance between two adjacent microvilli from 88.1 ± 15.9 nm in *WT* (Mean ± SD, n = 44) to 61.3 ± 7.8 nm in *cdh-8(ok628*, n = 32) or 51.0 ± 9.1 nm in *cdh-8 (cas1109*, n = 49) mutant animals (Fig. 3c, e, and Extended Data Fig. 2e), further demonstrating a role of nanovilli in spacing microvilli. Thus, we propose a microvilli division model through which nanovilli regulate microvilli formation: an existing microvillus divides from the tip to the base, generating two nascent microvilli, and nanovilli insert into the newly split microvilli to push them apart (Fig. 4d).

Live imaging of microvilli division

To test the microvilli division model directly, we developed a high-resolution live-cell imaging method to follow the dynamic microvilli assembly process in *C. elegans*. Fluorescence live-cell imaging recorded microvilli dynamics in cell cultures [24,25]; however, time-lapse visualization of microvilli in a living organism is challenging. The 88 nm intermicrovillar distance does not allow conventional confocal microscopy to resolve adjacent microvilli. Neither could the super-resolution imaging platform be applied because their limited working space does not determine the intestinal lumen structures, which is at least five μm inside the *C. elegans* cuticle. Using the Airyscan technology in a GFP::ERM-1 KI animal, we successfully resolved individual microvilli along the intestinal lumen in developing *C. elegans* larvae (Fig. 4e). Line scan from the microvillar top or bottom or the whole microvilli revealed separate fluorescence peaks, and the average distance between the peaks of adjacent microvilli is 201.0 ± 9.1 nm (Mean ± SD, n = 44, Fig. 4e), which is comparable to the measurements from the cryo-ET tomogram slice (205.8 ± 28.0 nm, Mean ± SD, n = 49). Time-lapse recording started from a Y-shaped microvillus (Fig. 4f, yellow dotted box), and its two tips gradually moved apart, forming a V-shaped microvillus (0.8 and 1.6 min in Fig. 4f). Eventually, two nascent microvilli were separated (Fig. 4f). A stick-like microvillus underwent a similar process to assemble two new microvilli, and the Y- or V-shaped microvilli were intermediate structures when a mother microvillus split into two daughter microvilli (Fig. 4g and more examples in Extended Data Fig. 4). Our live imaging data support the microvilli division model in which two nascent microvilli are generated by dividing an old microvillus. In this model, the daughter microvilli formation uses the mother microvilli as their templates, forming two daughter microvilli of identical sizes, reminiscent of chromosome or centriole duplication in a dividing cell. In support of microvilli duplication, the Y-shaped microvilli base contains more actin bundles and is larger than the regular stick-like microvilli (Fig. 4b, c).

Discussion

The microvilli division model raises many fascinating questions that await future investigations. For example, what is the signal that triggers microvilli division? How do new actin bundles grow and the microvillar size increase within the mother microvillus? How to split the mother microvillus from the tip? How to space two daughter microvilli? Our observation of nanovilli on the lateral surface of microvilli

offers a glimpse of microvilli spacing. The absence of nanovilli still permits microvilli formation, despite their Y-shaped morphology, suggesting that additional molecules may be involved in microvilli separation. The methodologies developed in this study will help us address these questions, and our understanding of microvilli division may benefit from the design principles underlying chromosome and centriole replication and separation during the cell cycle. The microvilli division model addresses how to assemble microvilli from existing ones during tissue homeostasis or late development, complementing a microvillar elongation strategy for *de novo* microvilli formation [1-3,25].

In addition to microvilli separation, the decoration of nanovilli on microvilli may have additional advantages. These appendages cover microvilli with such a high intensity that nanovilli help host defense against microbe infection. On the other hand, nanovilli decoration appears to be a paradox to microvilli's role in increasing surface area for nutrient uptake. Numerous nanovilli occupy microvilli's lateral surface, where food absorption occurs [3,4]. One possibility could be that nanovilli act as a food filter, selecting the predigested food particles whose sizes are smaller than the inter-nanovillar distance to contact the microvillar membrane. Without such a filter, the food particles of various sizes may occupy the membrane but cannot be absorbed efficiently, explaining the slow growth in *cdh-8* mutant larvae (Extended Data Fig. 3).

Taken together, we uncovered that nanovilli decorate the lateral surface of microvilli. We provide evidence that nanovilli are composed of a protocadherin protein and space microvilli. Our results suggest a microvilli division model that offers mechanistic insights into microvilli uniformity. Microvilli are widespread across species [1,3,4,14], and likewise, other animals may also develop nanovilli, the notion of which is supported by the similar decoration on the surface of mouse intestinal microvilli (Fig. 2b, c). Despite decades of ultrastructural studies by TEM, our research indicates that anatomical structures may be more complex and fascinating than is currently appreciated; given the power of the cryo-ET platform, perhaps nanovilli are the "tip of the iceberg," and additional biological structures will be uncovered *in situ*.

Declarations

Acknowledgments

We thank Drs. Mingjie Zhang, Piali Sengupta, Jianlin Lei, Hongwei Wang, Li Yu, Ye-Guang Chen, and Mark Mooseker for discussions; Caenorhabditis Genetics Center (CGC) for providing some strains; Tsinghua University Cryo-EM Facility of China National Center for Protein Sciences (Beijing) for high-pressure freezing, cryo-FIB milling, and tomography data collection. This work was supported by the National Key R&D Program of China (2019YFA0508401, 2017YFA0503501, and 2017YFA0102900) and the National Natural Science Foundation China (grants 31991190, 31730052, 31525015, 31861143042, 31561130153, 31671444, 31871352).

References

1 Crawley, S. W., Mooseker, M. S. & Tyska, M. J. Shaping the intestinal brush border. *J Cell Biol* **207**, 441-451, doi:10.1083/jcb.201407015 (2014).

2 Pelaseyed, T. & Bretscher, A. Regulation of actin-based apical structures on epithelial cells. *J Cell Sci* **131**, doi:10.1242/jcs.221853 (2018).

3 Sauvanet, C., Wayt, J., Pelaseyed, T. & Bretscher, A. Structure, regulation, and functional diversity of microvilli on the apical domain of epithelial cells. *Annu Rev Cell Dev Biol* **31**, 593-621, doi:10.1146/annurev-cellbio-100814-125234 (2015).

4 Delacour, D., Salomon, J., Robine, S. & Louvard, D. Plasticity of the brush border - the yin and yang of intestinal homeostasis. *Nat Rev Gastroenterol Hepatol* **13**, 161-174, doi:10.1038/nrgastro.2016.5 (2016).

5 Coudrier, E., Kerjaschki, D. & Louvard, D. Cytoskeleton organization and submembranous interactions in intestinal and renal brush borders. *Kidney Int* **34**, 309-320, doi:10.1038/ki.1988.183 (1988).

6 Schwander, M., Kachar, B. & Muller, U. Review series: The cell biology of hearing. *J Cell Biol* **190**, 9-20, doi:10.1083/jcb.201001138 (2010).

7 Gerbe, F. & Jay, P. Intestinal tuft cells: epithelial sentinels linking luminal cues to the immune system. *Mucosal Immunol* **9**, 1353-1359, doi:10.1038/mi.2016.68 (2016).

8 Krasteva, G. & Kummer, W. "Tasting" the airway lining fluid. *Histochem Cell Biol* **138**, 365-383, doi:10.1007/s00418-012-0993-5 (2012).

9 Kummer, W. & Deckmann, K. Brush cells, the newly identified gatekeepers of the urinary tract. *Curr Opin Urol* **27**, 85-92, doi:10.1097/MOU.0000000000000361 (2017).

10 Schneeberger, K., Roth, S., Nieuwenhuis, E. E. S. & Middendorp, S. Intestinal epithelial cell polarity defects in disease: lessons from microvillus inclusion disease. *Dis Model Mech* **11**, doi:10.1242/dmm.031088 (2018).

11 Gehart, H. & Clevers, H. Tales from the crypt: new insights into intestinal stem cells. *Nat Rev Gastroenterol Hepatol* **16**, 19-34, doi:10.1038/s41575-018-0081-y (2019).

12 Harapin, J. *et al.* Structural analysis of multicellular organisms with cryo-electron tomography. *Nat Methods* **12**, 634-636, doi:10.1038/nmeth.3401 (2015).

13 Mahamid, J. *et al.* Visualizing the molecular sociology at the HeLa cell nuclear periphery. *Science* **351**, 969-972, doi:10.1126/science.aad8857 (2016).

14 Dimov, I. & Maduro, M. F. The C. elegans intestine: organogenesis, digestion, and physiology. *Cell Tissue Res* **377**, 383-396, doi:10.1007/s00441-019-03036-4 (2019).

15 McGhee, J. D. The C. elegans intestine. *WormBook*, 1-36, doi:10.1895/wormbook.1.133.1 (2007).

16 Crawley, S. W. *et al.* Intestinal brush border assembly driven by protocadherin-based intermicrovillar adhesion. *Cell* **157**, 433-446, doi:10.1016/j.cell.2014.01.067 (2014).

17 McConnell, R. E., Benesh, A. E., Mao, S., Tabb, D. L. & Tyska, M. J. Proteomic analysis of the enterocyte brush border. *Am J Physiol Gastrointest Liver Physiol* **300**, G914-926, doi:10.1152/ajpgi.00005.2011 (2011).

18 D'Alterio, C. *et al.* Drosophila melanogaster Cad99C, the orthologue of human Usher cadherin PCDH15, regulates the length of microvilli. *J Cell Biol* **171**, 549-558, doi:10.1083/jcb.200507072 (2005).

19 Ge, J. *et al.* Structure of mouse protocadherin 15 of the stereocilia tip link in complex with LHFPL5. *Elife* **7**, doi:10.7554/eLife.38770 (2018).

20 Lefebvre, J. L., Kostadinov, D., Chen, W. V., Maniatis, T. & Sanes, J. R. Protocadherins mediate dendritic self-avoidance in the mammalian nervous system. *Nature* **488**, 517-521, doi:10.1038/nature11305 (2012).

21 Zipursky, S. L. & Grueber, W. B. The molecular basis of self-avoidance. *Annu Rev Neurosci* **36**, 547-568, doi:10.1146/annurev-neuro-062111-150414 (2013).

22 Araya-Secchi, R., Neel, B. L. & Sotomayor, M. An elastic element in the protocadherin-15 tip link of the inner ear. *Nat Commun* **7**, 13458, doi:10.1038/ncomms13458 (2016).

23 Tilney, L. G. & Cardell, R. R. Factors controlling the reassembly of the microvillous border of the small intestine of the salamander. *J Cell Biol* **47**, 408-422, doi:10.1083/jcb.47.2.408 (1970).

24 Postema, M. M., Grega-Larson, N. E., Neininger, A. C. & Tyska, M. J. IRTKS (BAIAP2L1) Elongates Epithelial Microvilli Using EPS8-Dependent and Independent Mechanisms. *Curr Biol* **28**, 2876-2888 e2874, doi:10.1016/j.cub.2018.07.022 (2018).

25 Meenderink, L. M. *et al.* Actin Dynamics Drive Microvillar Motility and Clustering during Brush Border Assembly. *Dev Cell* **50**, 545-556 e544, doi:10.1016/j.devcel.2019.07.008 (2019).

Figures

Figure 1

In situ cryo-ET of the C. elegans intestinal brush border reveals nanovilli on the lateral surface of microvilli. (a) A schematic diagram of an intestinal epithelial cell (left) and two microvilli (right) from the dotted box in the left. The glycocalyx and tip link are the characterized cell surface structure at microvillar tips. This work shows that numerous nanovilli (magenta) decorates the lateral surface of microvilli. (b) Representative cryo-SEM images of the C. elegans L1 larvae before and after FIB milling (left and

middle). Scale bars, 10 μm. Representative FIB image of the ~200-nm-thick cryo-lamella (right). Scale bars, 5 μm. (c) 3D rendering of the C. elegans intestinal brush border showing various macromolecules and structures. Magenta, nanovilli; cyan, membrane; yellow, actin; beige, ribosome; green, mitochondria; orange, endoplasmic reticulum (ER). Nanovilli and ribosomes were mapped back in the tomogram with the computed location and orientation. (d) A selected microvillus from (c) magnified for visualization. (e and f) Cryo-ET tomogram slices of microvilli (e, top view; f, side view). Scale bars in c-f, 50 nm.

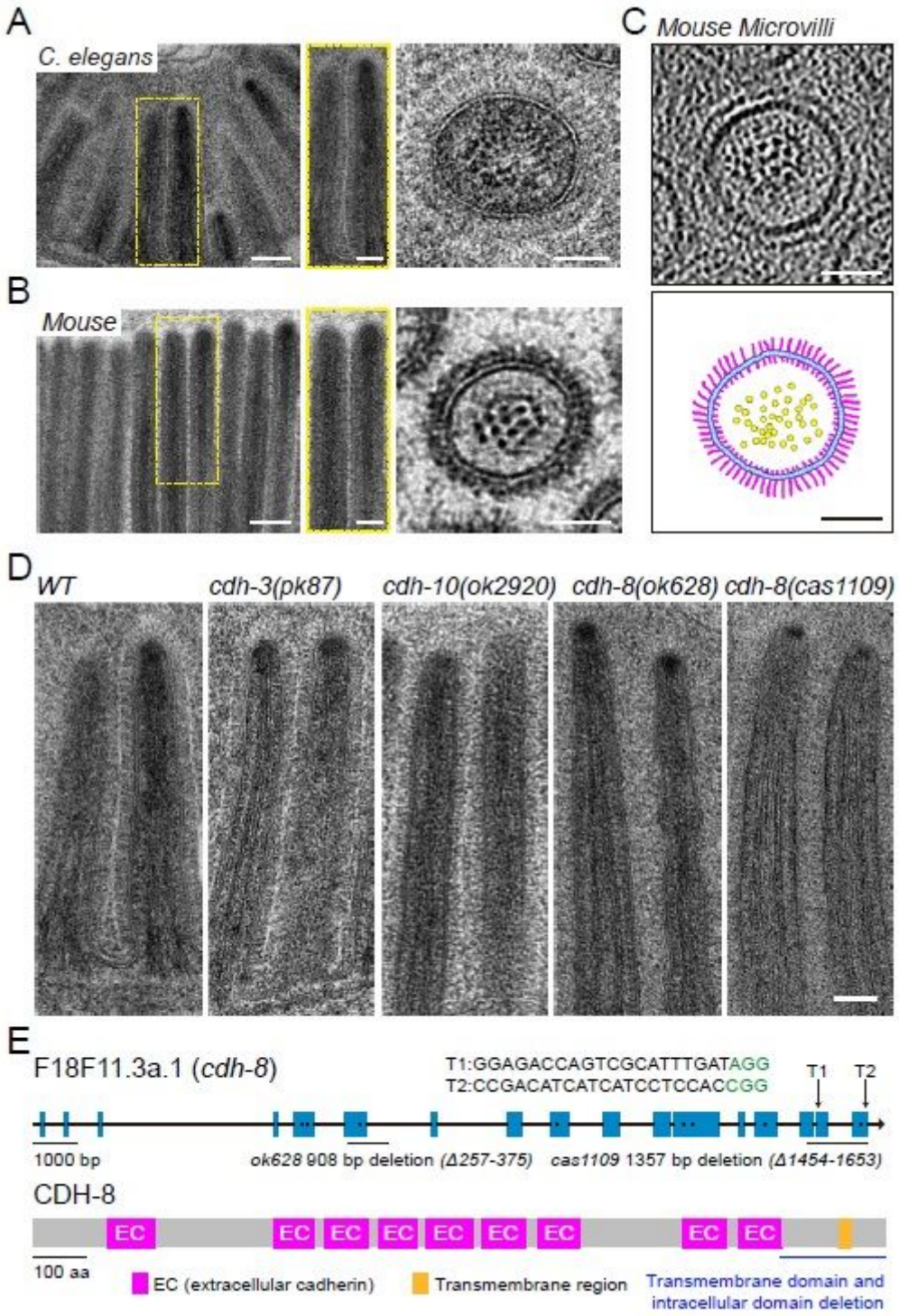

Figure 2

C. elegans microvilli in WT and cdh-8 mutant animals and mouse microvilli. (a) and (b) TEM of the longitudinal view of the C. elegans (a) and mouse (b) intestinal brush border (left). Yellow boxes on the middle are magnified images of the box on the left. Scale bars, 100 nm. High-magnification cross-section image of the C. elegans (a) and mouse (b) microvilli (right). Scale bars, 50 nm. (c) The cryo-ET tomogram slice of mouse microvilli (top) and the reconstruction of the plasma membrane, actin, and nanovilli (low). Scale bars, 50 nm. (d) TEM images of microvilli in WT, cdh-3(pk87), cdh-10(ok2920), cdh-8(ok628), and cdh-8(cas1109) mutant animals. Scale bar, 100 nm. (e) Gene structure of cdh-8 (Top). CRISPR-Cas9 generated the transmembrane and intracellular domain deletion allele (cas1109). Blue boxes represent exons. Arrow, sgRNA; green, PAM sequence. Schematics of the C. elegans CDH-8 protein (Bottom). Purple, cadherin extracellular domain; orange, transmembrane domain.

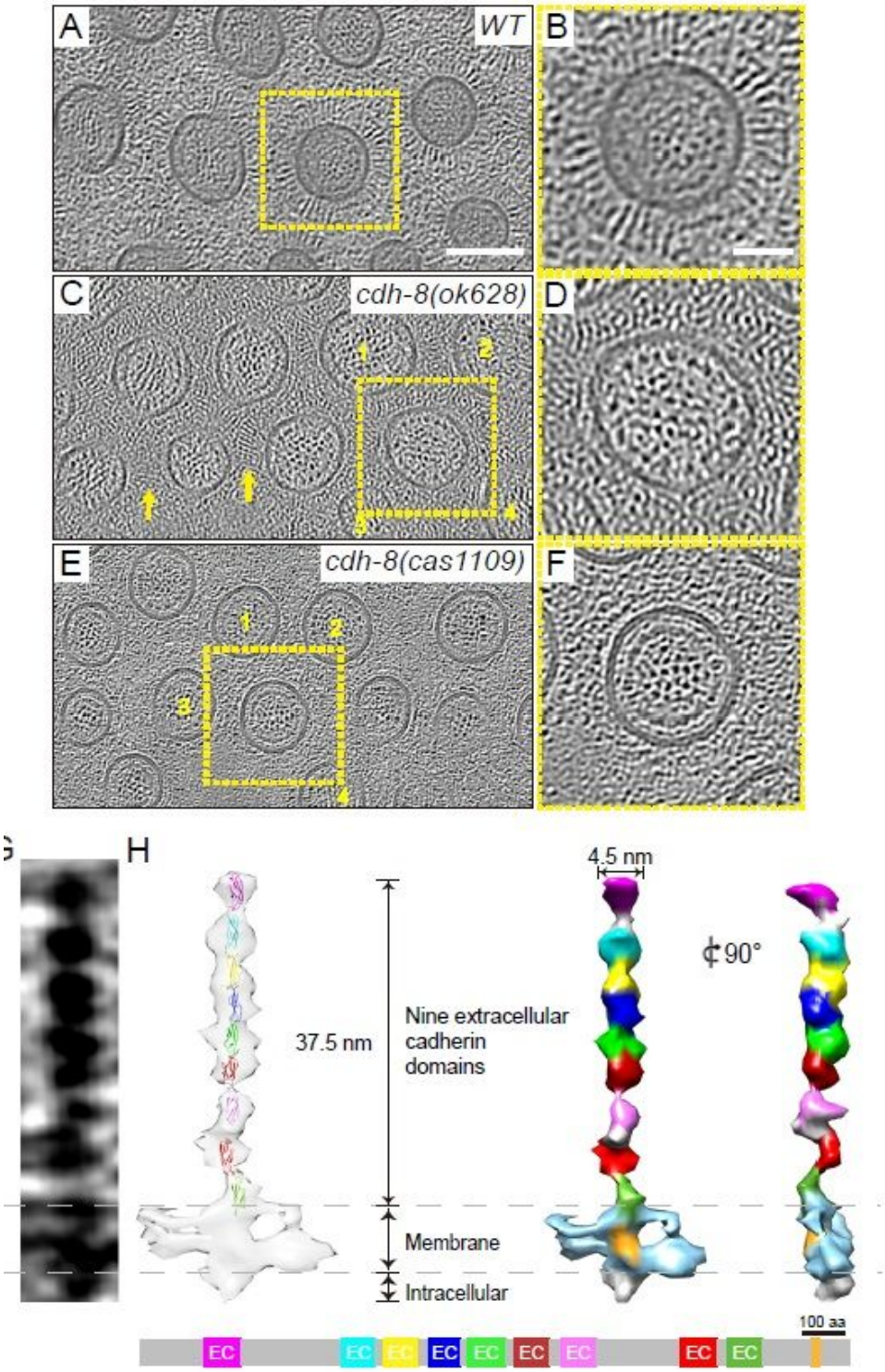

Figure 3

The CDH-8 protein and nanovilli. (a-f) Cryo-ET of the C. elegans intestinal brush border in WT (a and b), or cdh-8(ok628) (c and d); cdh-8(cas1109) (e and f). Microvilli were enlarged in the yellow boxes. The scale bar for (a), (c), and (e) represents 100 nm. The scale bar in the yellow box is 50 nm. The dotted yellow box in (a) did not contact neighboring microvilli in WT animals (the center of the box is the same as that of microvilli), whereas the same-sized box in cdh-8 mutant animals overlapped four adjacent microvilli in (c

and e). (g) Slice view of the sub-tomogram averaging structure of nanovilli. (h) The fitting model of the sub-tomogram averaging structure with the x-ray crystal structure of nine repeats of the EC8 domain of PCDH15 (PDB code, 4XHZ). Below is the schematic domain structure of CDH-8.

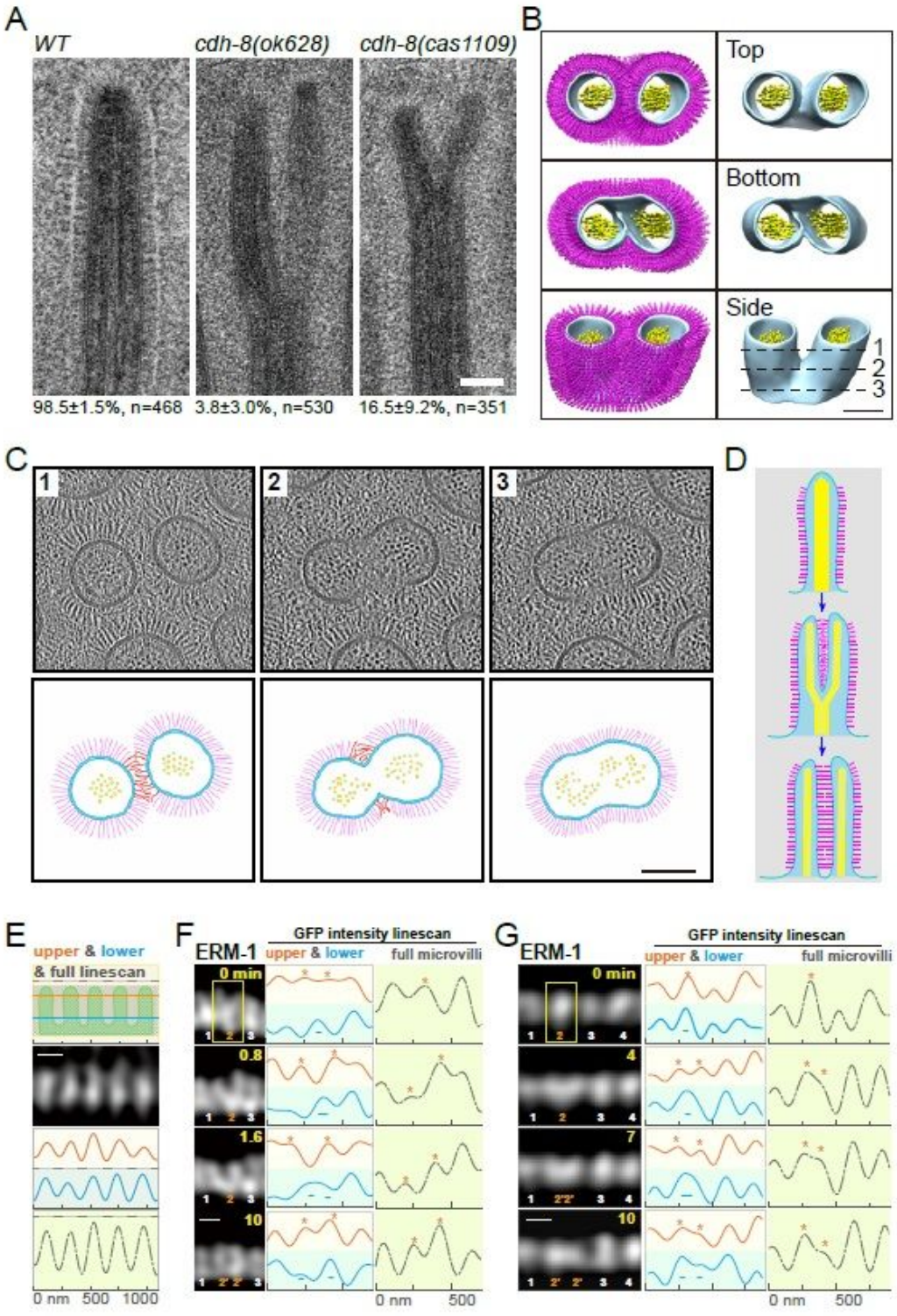

Figure 4

CDH-8 regulates microvillus assembly and a proposed model. (a) TEM images of microvilli in WT and the Y-shaped microvilli in cdh-8(ok628) and cdh-8(1109) mutants. Scale bar, 100 nm. Below were

percentages of the observed stick-like microvilli or Y-shaped microvilli. (b) The 3D reconstruction of the representative Y-shape microvilli in WT animals. Scale bar, 100 nm. (c) Cryo-ET tomogram slices of the Y-shape microvilli. Lines 1-3 in (b) indicate the localization for tomographic slices on the upper. The lower shows the schematic. Scale bar, 100 nm. (d) A proposed role of nanovilli in microvilli division. Nanovilli, magenta; actin in microvilli, yellow; plasma membrane, cyan. (e) Schematics of high-resolution live-cell imaging of microvilli in a developing C. elegans larva using the Airyscan confocal microscopy. In the first row, the orange line (40 nm below the top of microvilli), the blue line (40 nm above the bottom of microvilli), and the grey bar (the entire microvilli) indicate the line scan for measuring the fluorescence intensity from microvilli images (ERM-1::GFP) in the second row or (f) and (g). (f, g) Time-lapse fluorescence images of a Y-shaped microvillus (f) or a stick-like microvillus (g) separation into two nascent microvilli. The yellow boxes, asters, and "-" show the #2 microvillus separation, whereas other microvilli remained unchanged.

Supplementary Files

This is a list of supplementary files associated with this preprint. Click to download.

- 20210406nanovilliMM.docx
- Tables1.xlsx
- 20210406Tables24.docx
- Video1.mp4
- Video2.mp4
- Video3.mp4
- Video4.mp4
- Video5.mp4
- Video6.mp4
- Video7.mp4
- SupplementaryFigures.pdf